sustainability

MDPI

Article

Design and Test for a New Type of Permanent Magnet Synchronous Generator Applied in Tidal Current Energy System

Yuxiang Zhao [1,2], Caixia Mo [1,2], Wanqiang Zhu [1,2,*], Jianmei Chen [1,2], Baigong Wu [3], Xiao Zhang [4], Xueming Zhang [1,2] and Liwei Chen [5]

[1] School of Physics, Northeast Normal University, 5268 Renmin Street, Changchun 130024, China
[2] Jilin Provincial Key Laboratory of Advanced Energy Development and Application Innovation, 5268 Renmin Street, Changchun 130024, China
[3] Marine Equipment and Technology Institute, Jiangsu University of Science and Technology, Zhenjiang 212000, China
[4] School of Energy and Power Engineering, Changchun Institute of Technology, Changchun 130012, China
[5] Hangzhou Jianghe Hydro-Electric Science & Technology Co., Ltd., Hangzhou 310012, China
* Correspondence: zhuwq773@nenu.edu.cn

Abstract: This article takes a 120 W direct-drive permanent magnet synchronous generator (PMSG) for tidal current energy as the research object, with the aim of starting at low flow velocity, low voltage regulation, and high sealing performance. The research was conducted on the design method of the generator, and the parameter calculation formula is modified based on the structural characteristics of the generator. The design scheme is simulated using the finite element method, and the voltage regulation is optimized using evolutionary algorithm. A prototype was manufactured based on the optimized scheme, and drag experiments and sealing tests were conducted. After that, the generator and impeller were assembled, and water tank drag experiments were conducted. The experimental results verified the reliability of the motor design method in this paper.

Keywords: tidal current energy; permanent magnet synchronous generator; finite element simulation; genetic algorithm; sealing test

Citation: Zhao, Y.; Mo, C.; Zhu, W.; Chen, J.; Wu, B.; Zhang, X.; Zhang, X.; Chen, L. Design and Test for a New Type of Permanent Magnet Synchronous Generator Applied in Tidal Current Energy System. *Sustainability* **2023**, *15*, 7378. https://doi.org/10.3390/su15097378

Academic Editor: Grigorios L. Kyriakopoulos

Received: 6 March 2023
Revised: 9 April 2023
Accepted: 25 April 2023
Published: 28 April 2023

1. Introduction

As fossil fuels continue to deplete and environmental issues gain more attention, there is a growing global focus on finding clean and renewable energy sources to replace traditional fossil fuels [1]. Tidal current energy is a kind of kinetic energy produced by the periodic horizontal movement of seawater, which is caused by the gravitational pull of the sun and moon. China possesses a significant amount of tidal current energy resources, which has become a topic of interest for many domestic research institutions [2].

The power generation cost of tidal power generation devices decreases with the increase of installed capacity. Research has shown that, when the installed capacity reaches 100 MW, the cost of tidal power generation will be highly competitive compared to traditional power generation models. This power generation method will become an effective supplement to traditional power generation methods and will ultimately partially replace traditional power generation.

Tidal current power generation was first researched in coastal countries in Europe. In 2015, the 1 MW project prototype designed by the Italian National Institute of Ocean Engineering was installed in Canada's Bay of Fundy [3]. In 2017, the HS1500 horizontal shaft unit (1.5 MW) designed by Atlantis Resources UK was installed in relevant sea areas and realized grid connection operation [4]. China has increased investment in tidal current power generation technology since the beginning of the 21st century. In April 2002, the "Wanxiang I" tidal current power generation device (70 kW) was researched

and built by Harbin Engineering University; it was then installed in Guishan waterway for a test operation [5]. In 2013, Northeast Normal University began to research and design a 300 kW horizontal-axis self-variable pitch project prototype, which was the first time that passive automatic pitch angles adjustment technology had been applied to tidal power generation [6]. In 2017, Zhejiang University designed the 650 kW horizontal-axis tidal current power generation device, which was successfully connected to the grid in Zhoushan [7].

In terms of generator design, Moury et al. proposed a permanent magnet synchronous generator with axial permanent magnet structure, which is complex in structure and high in cost [8]. Lindh et al. compared the difference between the surface-mounted and the embedded permanent magnet structures, then proposed a type of new embedded structure, but the new structure was complex and inconvenient to install [9]. Fizari et al. proposed a method to design a 1.5 kW PMSG that required low-speed starting performance and high reliability. Maxwell design software was used to obtain the parameter design results with 20 poles and 30 slots [10]. Nikbakhsh et al. first introduced the analysis, calculation, and design process of the PMSG, and used the ant colony optimization algorithm to optimize the design. The optimized design improves the efficiency and reduces the volume [11]. Quintal Palomo et al. conducted a finite element analysis of a surface-mounted PMSG. To obtain the lowest total harmonic distortion and cogging torque under the highest induced voltage, several optimization tests were conducted [12]. Faiz et al. introduced the design process of a three-phase PMSG for wind power generation. The AINiCo permanent magnetic material with low coercivity was used to replace the ordinary and expensive NdFeB permanent magnetic material. To reduce the cogging torque and improve the generator performance, the optimal number of cogging and magnetic poles was determined [13].

After analyzing various power generation devices and design methods, it becomes clear that there is currently no research dedicated to underwater generators specifically designed for low-speed tidal current. This paper presents a design model for an underwater generator with large air gap that takes into consideration the low-speed start, large torque and insulation sealing characteristics applied in tidal current energy system. The design is evaluated through simulation analysis, and a prototype is manufactured based on the evolutionary algorithms optimization results for reduce the voltage regulation, a kind of underwater centrifugal sealing technology is used to seal the generator. A pool drag experiment is conducted to test the prototype's ability to verify the low-speed starting performance of the generator. The experimental results demonstrate the effectiveness of the design and sealing methods for tidal current energy PMSG presented in this paper.

2. Underwater Generator Design

2.1. Generator Specifications

The primary dimensions of the generator include the outer diameter (D_{il}) of the armature near the air gap and the effective length (L_{ef}) of the iron core. To determine the main dimensions of the generator, it is necessary to first identify the rated parameters [14]. The rated parameters of the generator are shown in Table 1.

Table 1. Rated parameters of the generator.

Rated Power	Rated Voltage	Rated Current	Rated Rotation Speed
120 W	36 V	1.93 A	28 r/min

2.2. Generator Primary Dimensions

The generator adopts an embedded magnetic pole structure on the surface of the outer rotor. To preliminarily determine the primary dimensions of the generator, the calculated power P' shall be calculated according to Formula (1) based on the rated power P_N.

$$P' = \frac{K_E P_N}{\cos \varphi_N} \quad (1)$$

where K_E is ratio of induced potential and terminal voltage at rated load, $\cos\varphi_N$ is power factor at rated load.

Because the underwater sealing performance of the generator needs to be considered, the thickness of the sealant layer on the stator surface should be reserved [15] when designing the air gap length. By referencing the primary dimension formula used for the traditional motor, the primary dimension formula of the tidal current energy PMSG is modified as follows:

$$\frac{D_{il}{}^2 L_{ef} n}{P'} = \frac{\alpha_{xz} 6.1 \times 10^4}{\alpha'_p K_{Nm} K_{dp} A B_\delta} = C_A \tag{2}$$

where n is generator rotation speed, α'_P is calculated pole arc coefficient, K_{Nm} is air gap magnetic field waveform coefficient, K_{dp} is armature winding coefficient, A is line load, B_δ is maximum value of air gap magnetic density. α_{xz} is air gap correction coefficient, which is used to correct the influence of the sealant layer on the air gap length.

The variation range of K_{Nm} and K_{dp} is small, the electromagnetic loads A and B_δ are selected according to experience, and the approximate value $D_{il}{}^2 L_{ef}$ of the effective volume can be determined by Formula (2). However, the same value of the effective volume could have different shapes. In order to reflect the geometric shape of the generator, the main dimension ratio λ is introduced. The expression of λ is Formula (3).

$$\lambda = \frac{L_{ef}}{\tau} \tag{3}$$

where τ is polar distance. Select the right λ and the armature outer diameter D_{il}, value then the effective length of iron core L_{ef} could be preliminarily determined.

2.3. Size of Permanent Magnets

The permanent magnet size includes the axial length L_M, radial magnetization length h_M, and area S_M. L_M is slightly smaller than the axial length of the generator core, so only the radial magnetization length h_M and area S_M need to be designed. These two parameters can be obtained from Formulas (4) and (5) [16].

$$h_M = \frac{2 k_\alpha k_\delta b_{m0} \delta}{(1 - b_{m0}) \sigma_0} \tag{4}$$

$$S_M = \frac{2 \sigma B_\delta S_\delta}{B_r} \tag{5}$$

where k_α is the rotor structure coefficient, k_δ is the saturation coefficient, and b_{m0} is the estimated value of permanent magnet no-load working point, δ is air gap length, σ_0 is the no-load magnetic leakage coefficient, σ is the magnetic leakage coefficient, B_δ is the air gap magnetic density, S_δ is the air gap area, and B_r is the remanence.

2.4. Number of Stator Slot

Once the number of poles and phases are established, the number of stator slots is determined by the number of slots q for per pole and phase. Tidal current energy PMSG operates at low speed, so it requires multi-pole structure, which influences the parameter q. However, choosing an integer value for q could cause an increase in the cogging torque and electromagnetic loss. Therefore, the generator adopts fractional slot winding design, and the number of slots q per pole and phase can be found using Formula (6).

$$q = \frac{Z}{2pm} = b + \frac{c}{d} = b + \frac{e}{2p} \tag{6}$$

where Z is the number of stator slots, p is the number of pole pairs, m is the number of phases, b is an integer.

2.5. Winding Design

The induced voltage can be calculated using Formula (7):

$$E = 4.44Nf\phi_g \tag{7}$$

where N is the number of turns, f is the frequency of generator, Φ_g is the magnetic flux of each pole, which can be obtained from Formula (8):

$$\phi_g = \frac{2\pi R_g L_{ef} B_g}{2p} \tag{8}$$

where R_g is the average air gap radius and B_g is the air gap magnetic flux density.

According to the selected current density J and rated current I, the conductor area and diameter can be calculated using Formulas (9) and (10):

$$A_\omega = \frac{I}{J} \tag{9}$$

$$d_\omega = \sqrt{\frac{4A_\omega}{\pi}} \tag{10}$$

2.6. Generator Design Parameters

The basic parameters of the generator calculated according to the above formulas and experience are shown in Table 2:

Table 2. Generator design parameters.

Pole Number	Slot Number	Rotor External Diameter	Stator External Diameter	Stator Bore	Air Gap Length	Core Length	Permanent Magnet Thickness	Pole Arc Coefficient
40	72	620 mm	590 mm	476 mm	2.5 mm	25 mm	5 mm	0.94

3. Finite Element Simulation Analysis

3.1. Simulation Modeling

Ansoft Maxwell software adopts finite element discrete form to transform electromagnetic field calculation in engineering into huge matrix solutions [17]. This paper uses the RMxprt module in Ansoft Maxwell to establish a PMSG model for simulation analysis and imports the prototype model into the Maxwell 2D environment [18]. The established generator quarter model is shown in Figure 1, and the winding arrangement of the generator is shown in Figure 2.

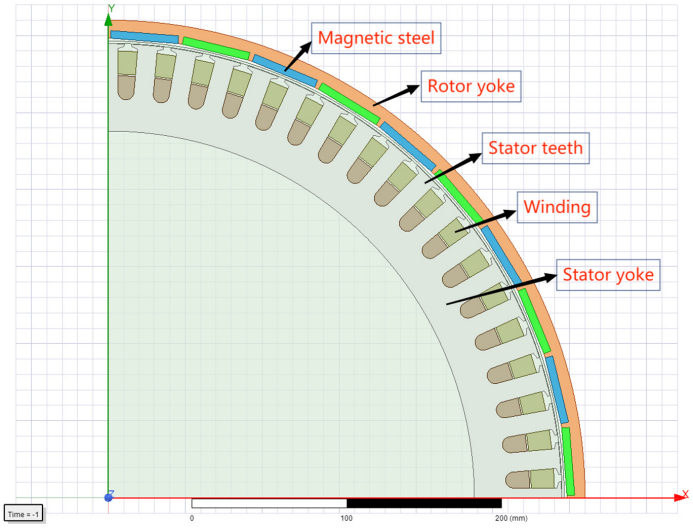

Figure 1. Generator quarter model.

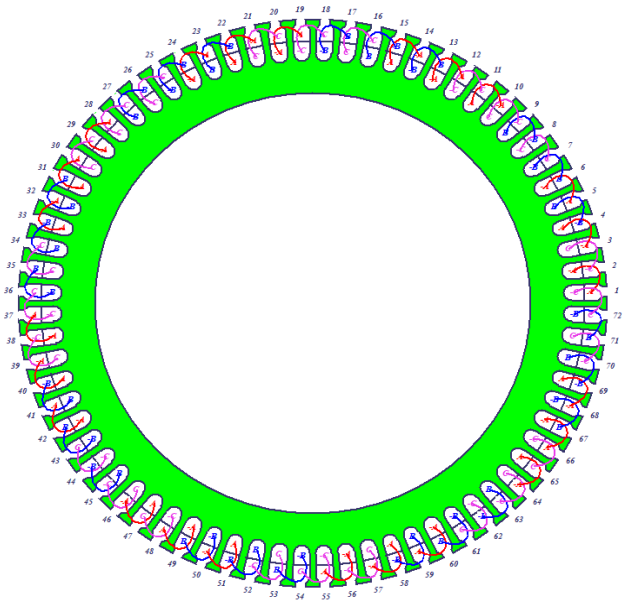

Figure 2. Winding arrangement diagram.

3.2. No-Load Simulation Analysis

The simplest operating mode of the PMSG is the no-load mode, where the air gap magnetic field is provided solely by the permanent magnet. Analyzing the no-load operation is a crucial step in verifying whether the generator performance meets standards and the magnetic circuit design is reasonable. For conducting no-load analysis, the model excitation source is selected as current source, and the current value is set to 0 A. The simulation results are presented In Figure 3. As shown in Figure 3, the magnetic density distribution is reasonable when the generator operates under no load, and there are no oversaturation points. Additionally, the distribution of magnetic field lines is uniform, and the magnetic leakage of the permanent magnet is small. As shown in Figure 4, the no-load voltage waveform is close to a sine wave, and the maximum phase voltage $U_{\max}$ is 30.6 V. According to Formula (11):

$$U_e = 1.225U_{\max} \tag{11}$$

where U_e is the rated voltage, the no-load simulation line voltage is 37.5 V, which is close to the designed rated voltage of 36 V.

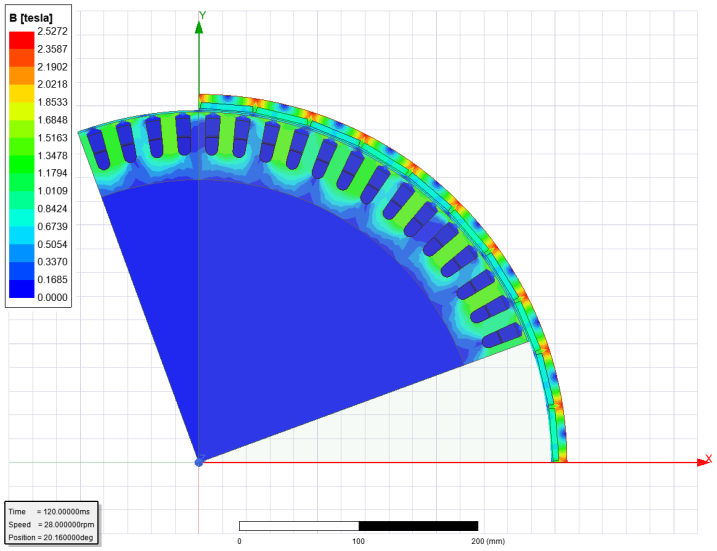

Figure 3. No load magnetic cloud diagram of generator.

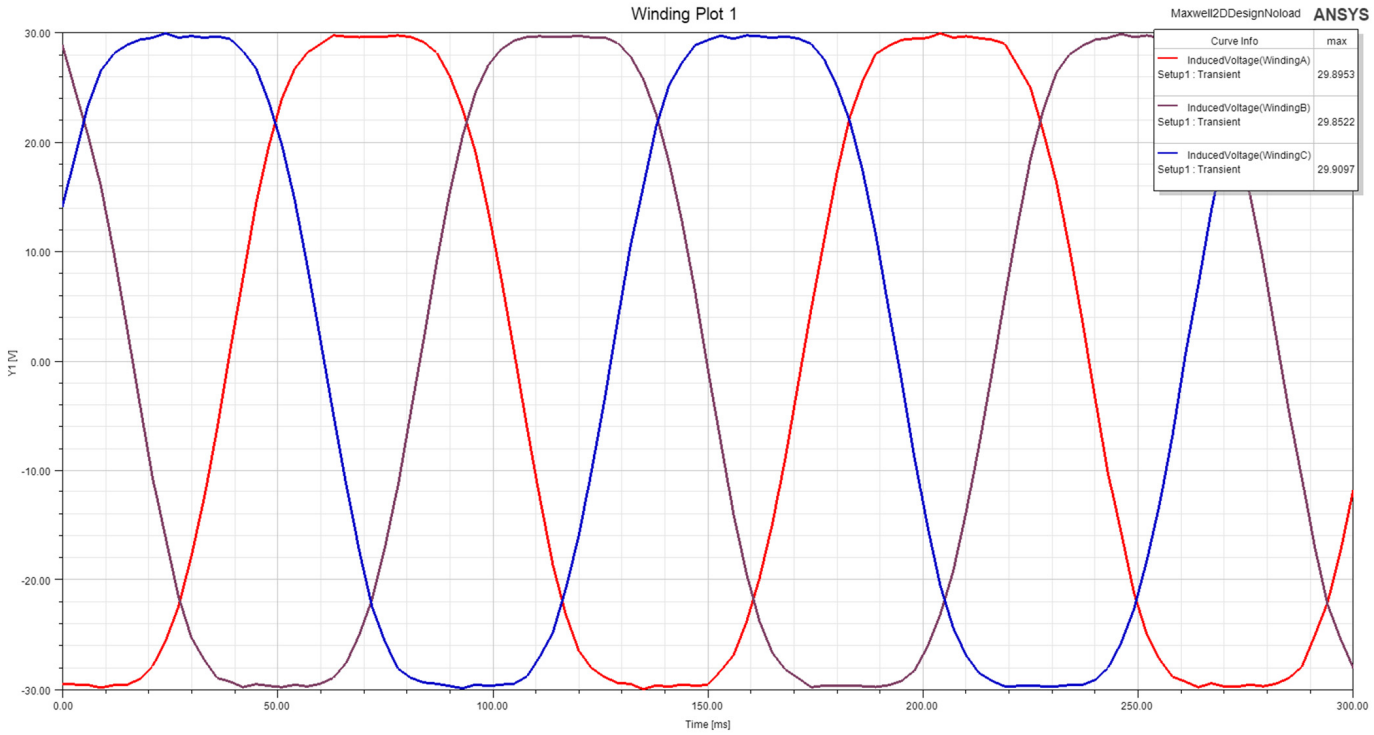

Figure 4. No load induced voltage of generator.

It can be seen from Figure 5 that the maximum cogging torque of the generator is 0.84 N·m, but that it is only 2% of the rated torque, which can meet the design requirements.

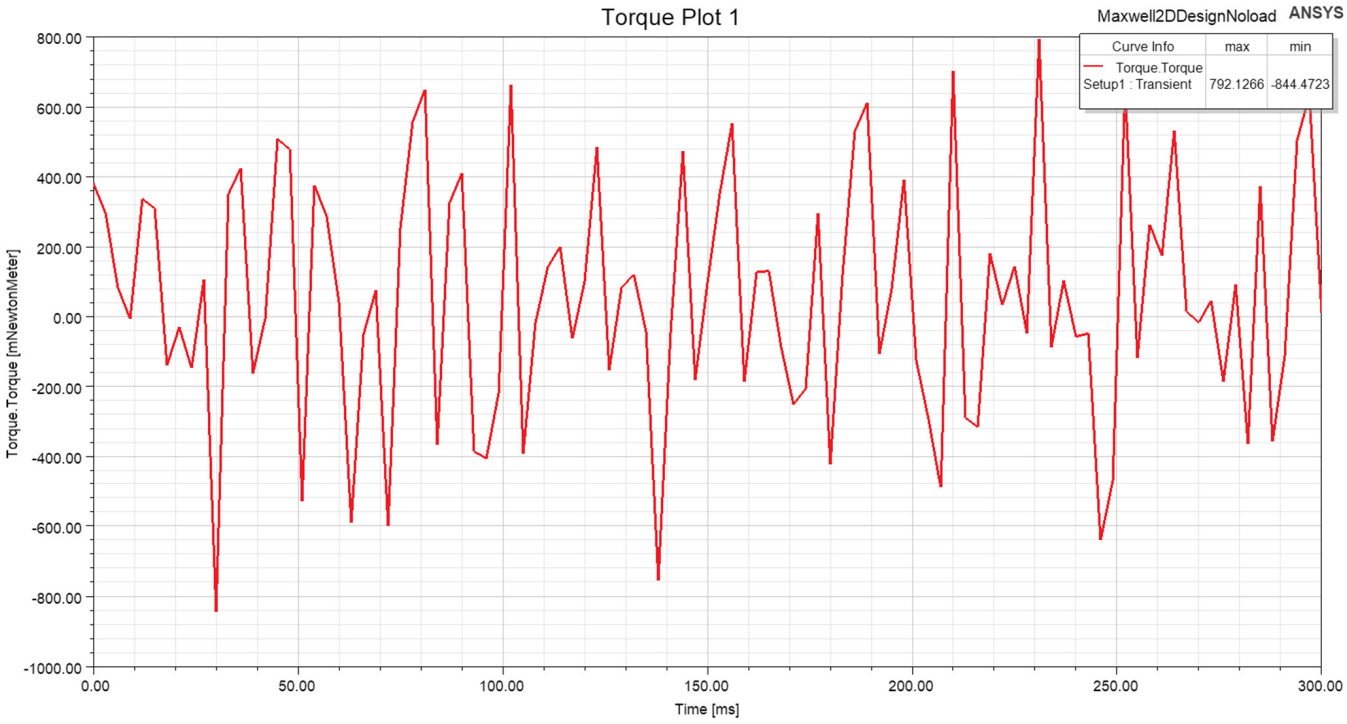

Figure 5. No load cogging torque of generator.

3.3. Load Simulation Analysis

By constructing the external circuit model of the generator, it is possible to simulate and analyze the generator at rated load. The load is a pure resistive load of 22.8 Ω. The results of the load simulation are presented in Figures 6–9. Figure 6 shows that there are no oversaturation points in the magnetic density of the generator during load operation. Figure 7 shows that the maximum load-induced phase voltage of the generator is 29.8 V, and according to Formula (11), the load simulation line voltage is 36.5 V, satisfying the design requirement of 36 V rated voltage. Figure 8 shows that the maximum load-induced current of the generator is 2.63 A, which matches the design requirement of 1.93 A rated current. Figure 9 shows that the load torque of the generator is 42 N·m, according to Formula (12):

$$T = \frac{9550P}{n} \tag{12}$$

where T is torque, P is rated power, and n is rated rotation speed. The simulation result is close to the calculated value of 41 N·m.

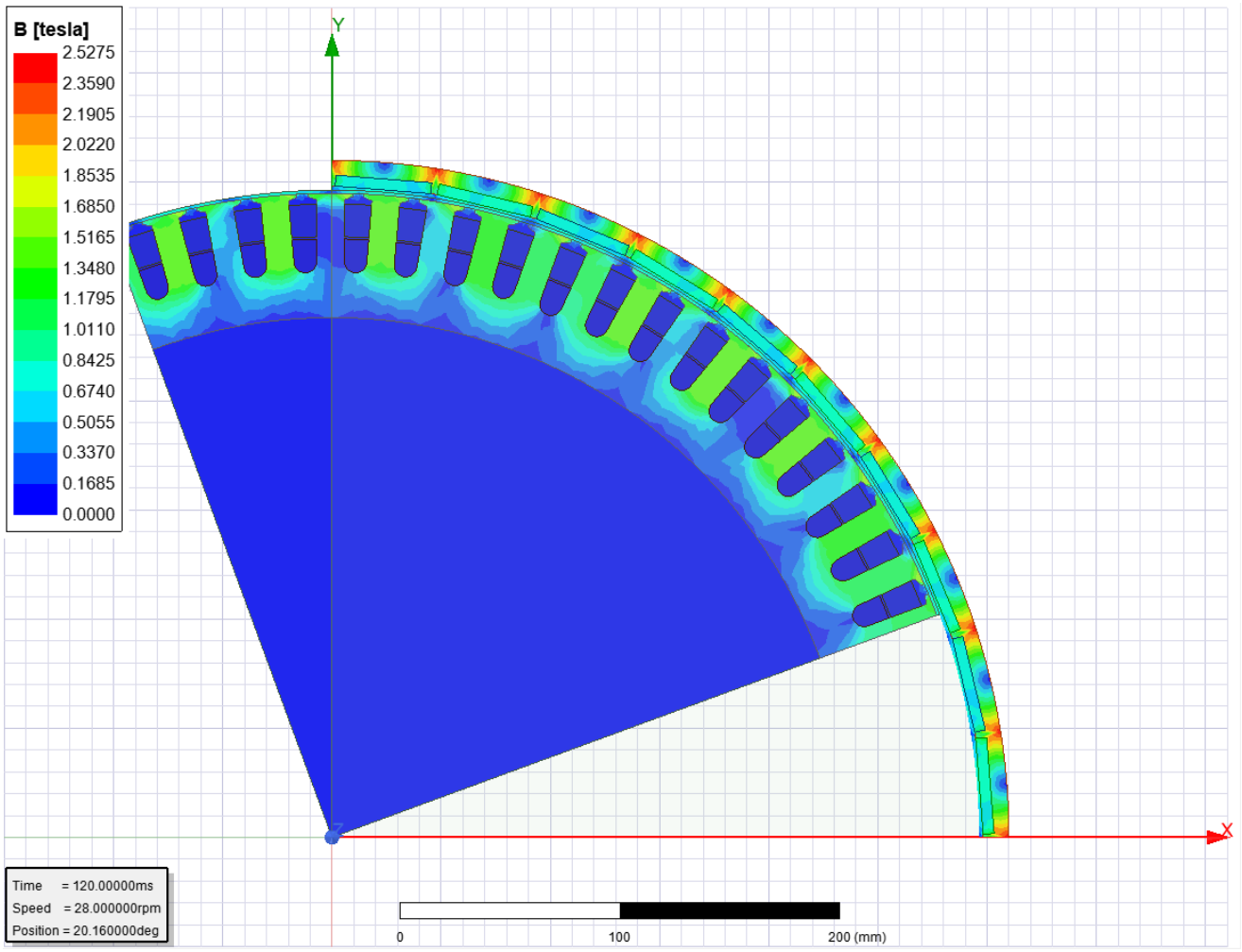

Figure 6. Load magnetic cloud diagram of generator.

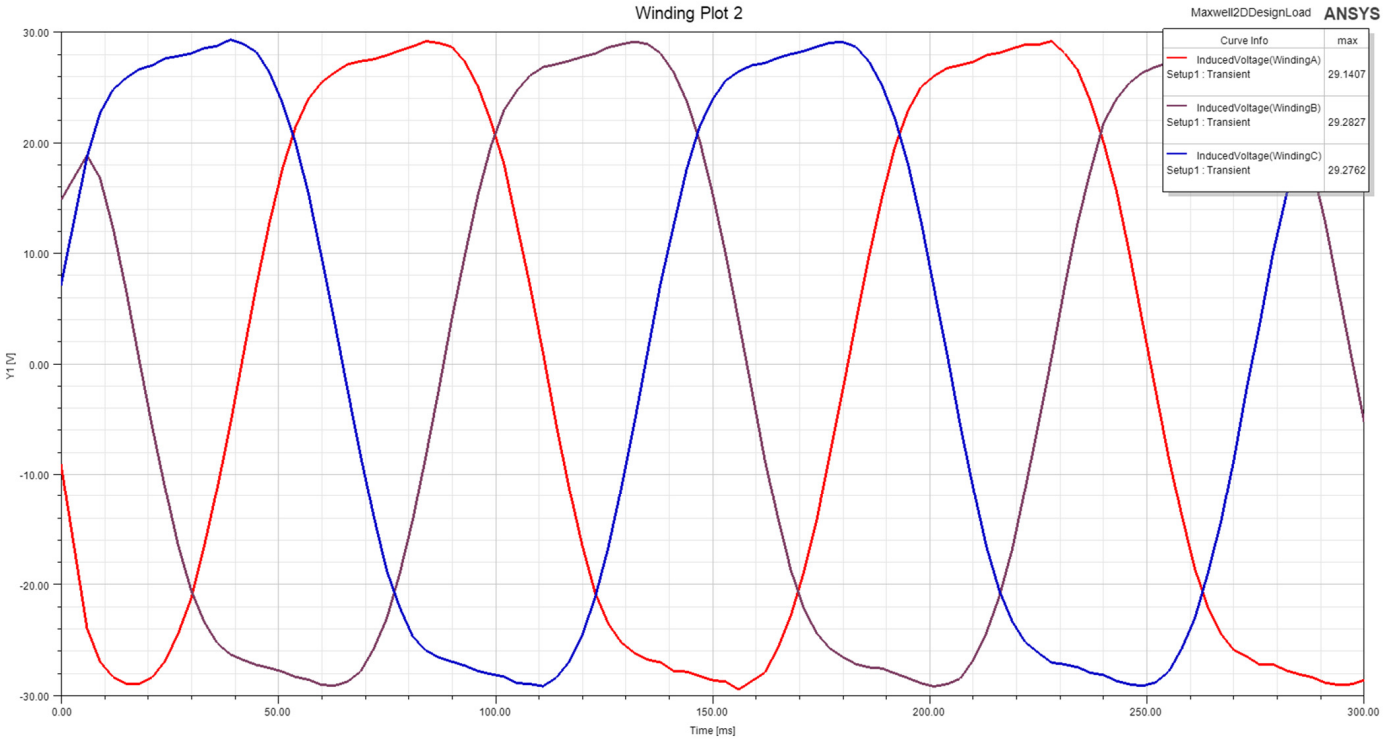

Figure 7. Load induced voltage of generator.

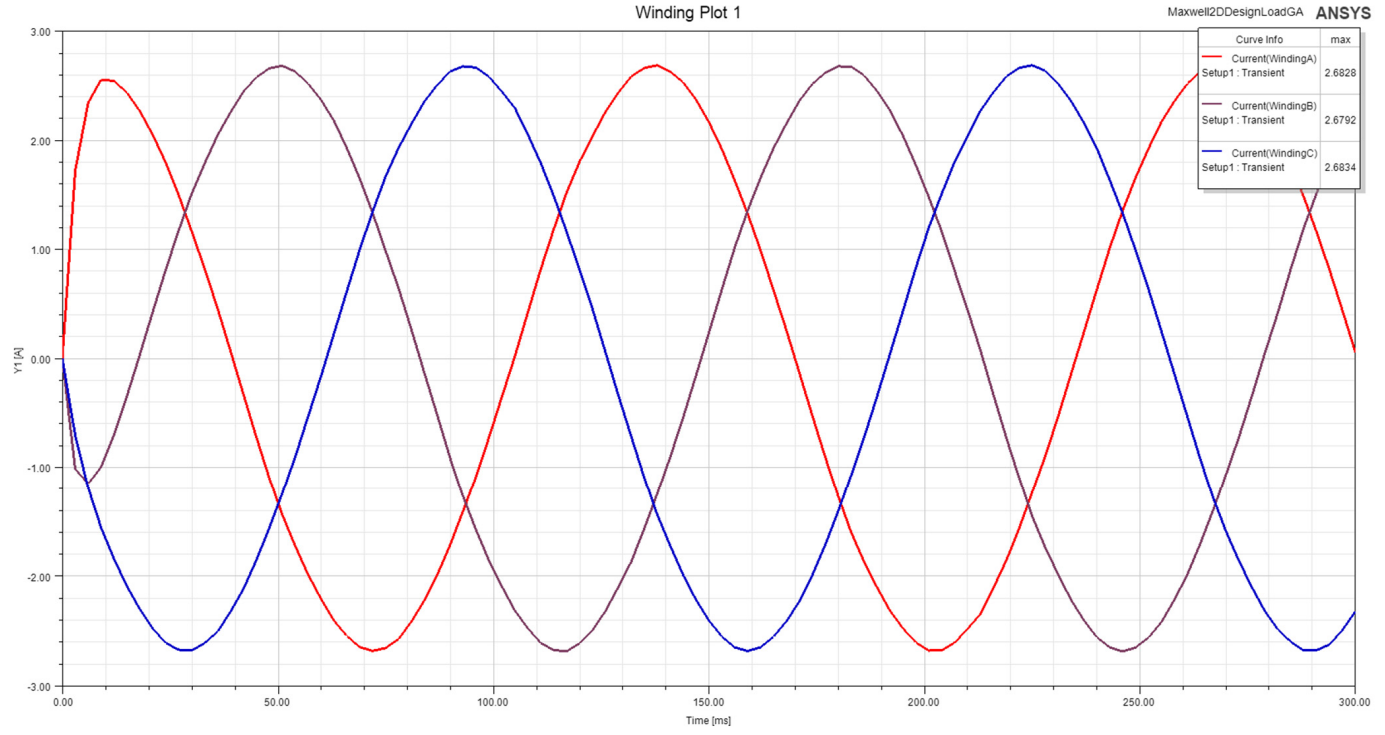

Figure 8. Line current of generator.

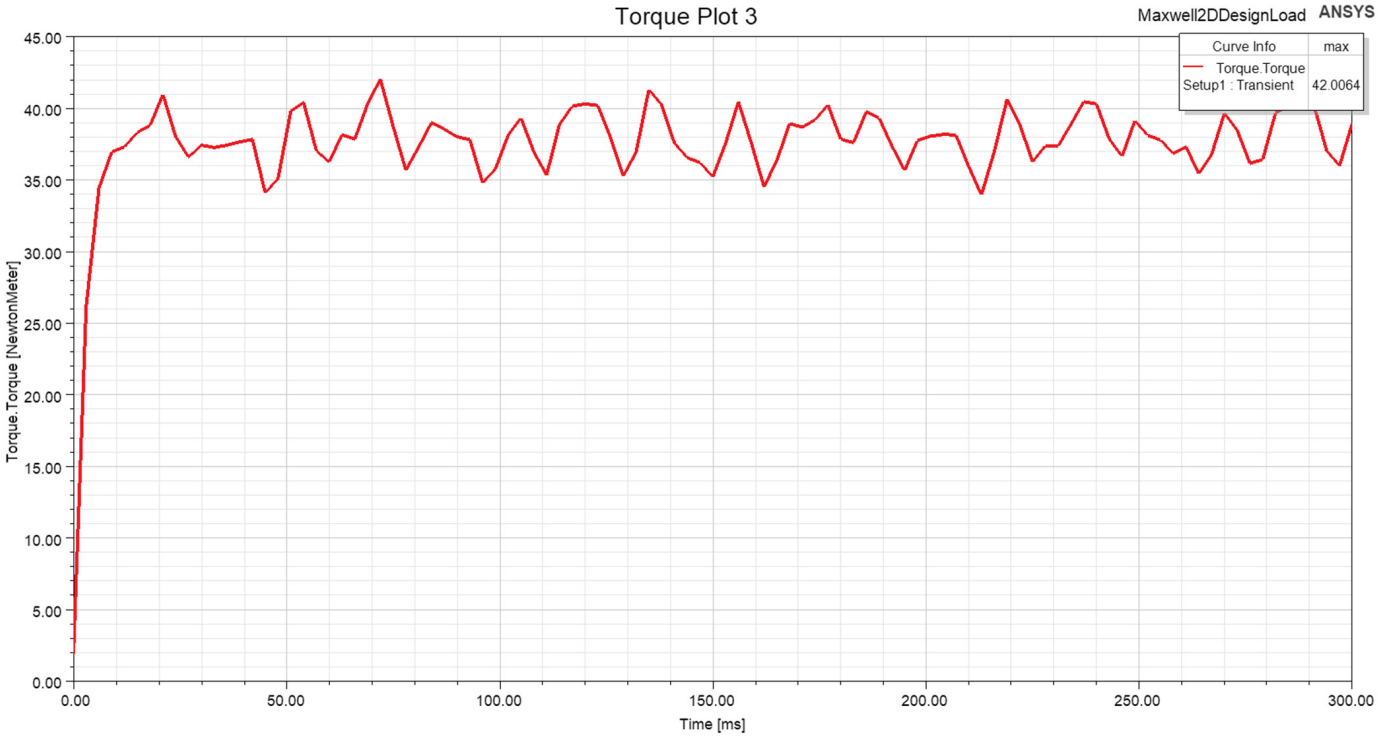

Figure 9. Load cogging torque of generator.

4. Genetic Algorithm Optimization of Generator Parameters

4.1. Analysis of the Voltage Regulation

Voltage regulation ΔU represents the change of output voltage when the load changes. Its value depends entirely on the basic characteristics of the generator itself, and its expression is:

$$\Delta U = \frac{E_0 - U}{U_N} \times 100\% \tag{13}$$

where E_0 is the no-load induced voltage, U is the output voltage, and U_N is the rated voltage.

Since it is difficult to adjust the air gap magnetic field after the PMSG is made, it is necessary to consider how to reduce ΔU at the design stage. The motor parameters, such as synchronous reactance X_q and X_d, armature winding resistance R_1, and leakage reactance X_1 must be reasonably designed at each phase. The specific factors that affect the above parameters are air gap length, iron core length, permanent magnet magnetization direction length, and stator slot size. Therefore, the influence of each parameter on the voltage regulation is analyzed below [19].

4.1.1. Effect of Air Gap Length

The approximate calculation formula of quadrature axis armature reaction reactance X_{aq} of PMSG is:

$$X_{aq} = \frac{E_0 F_{aq}}{I_N F_\delta} K_{aq} \frac{1}{1 + \frac{b_M}{2\mu_r \delta K_\delta}} \tag{14}$$

where F_{aq} is quadrature axis armature magnetomotive force, F_δ is air gap magnetic potential difference, K_{aq} is the conversion coefficient of the quadrature axis armature magnetomotive force, b_M is permanent magnet width, μ_r is the relative recovery permeability of the permanent magnet, δ is air gap length, and K_δ is air gap coefficient. The air gap length can be determined by the above formula.

4.1.2. Effect of Core Length

Under the rated load, the PMSG's direct axis electromotive force (E_d) and quadrature axis armature reactance (X_{aq}) are both correlated to axial length (L_M) of the permanent magnet and calculated length (L_{ef}) of the armature. The expressions are:

$$E_d = 4.44 f_1 N K_{dp} K_\phi \phi_{\delta N} \tag{15}$$

$$\phi_{\delta N} = (b_{mN} - h_{mN}\lambda_\sigma) B_r A_m \times 10^{-4} \tag{16}$$

$$X_{aq} = \frac{2}{\pi} L_{ef} \tau K_{dp} N \frac{B_{aq1}}{I_q} \tag{17}$$

$$L_{ef} = L_1 + 2\delta \tag{18}$$

where $A_m = b_M L_M$, L_1 is the length of stator core. The axial length L_M of the permanent magnet is equal to L_1. It can be seen that L_1 can directly affect E_d and X_{aq}.

4.1.3. Effect of Permanent Magnet Magnetization Direction Length

When the PMSG is under rated load, the relationship between E_d and permanent magnet thickness h_{Mp} is as follows:

$$b_{mN} = \varphi_{mN} = \frac{\lambda_n (1 - f')}{\lambda_n + 1} \tag{19}$$

$$h_{mN} = f_{mN} = \frac{\lambda_n f' + 1}{\lambda_n + 1} \tag{20}$$

$$f' = \frac{F_{ad}}{\sigma_0 H_c h_{Mp} \times 10^{-2}} \tag{21}$$

where λ_N is the composite magnetic guide unit value of the external magnetic circuit, σ_0 is no-load magnetic leakage coefficient, and F_{ad} is direct axis armature magnetomotive force. It can be seen that h_{Mp} can change the voltage regulation by influencing the direct axis electromotive force E_d.

4.1.4. Effect of Stator Slot Size

The calculation formula of each phase armature winding leakage reactance X_1 is as follows:

$$X_1 = 15.5 \frac{f}{100} \left(\frac{N}{100}\right)^2 \frac{L_1}{pq} \sum \lambda \times 10^{-2} \tag{22}$$

where λ is the total magnetic leakage permeability, and its expression is:

$$\sum \lambda = \lambda_t + \lambda_d + \lambda_E + \lambda_s \tag{23}$$

where λ_t is tooth-tip-specific magnetic leakage conductance, λ_d is differential leakage permeance, λ_E is the specific leakage magnetic conductivity at the end, λ_S is slot-specific magnetic permeability [20]. The slot-specific magnetic leakage conductance is mainly affected by the stator slot type, and its expression is:

$$\lambda_s = \frac{1}{4}\left[0.31 + \frac{2h_1}{3(d_2 + b)} + \frac{h_2}{b} + \frac{k_1 h_3}{b + d_1} + k_2\left(0.985 + \frac{h_5}{b_0}\right)\right] \tag{24}$$

The specific meaning of the parameter is shown in Figure 10.

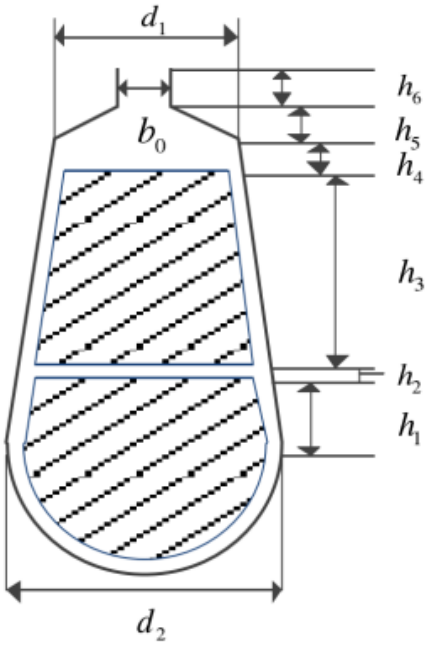

Figure 10. Stator slot size parameters.

It can be seen from the above formulas that the stator slot size changes the voltage regulation by affecting the winding leakage reactance X_1.

4.2. Voltage Regulation Genetic Algorithm Optimization

Select air gap length δ, core length L_1, permanent magnet thickness h_{Mp}, slot width b_0, slot body width d_2 and slot depth h as optimization variables, and the objective function expression to be optimized is:

$$f(x) = Min[\Delta U(\sigma, L_1, h_{Mp}, b_0, d_2, h)] \tag{25}$$

The genetic algorithm parameters are shown in Table 3, the range of optimization variables are shown in Table 4, and the optimization results are shown in Table 5. The effect of air gap length, iron core length, and permanent magnet thickness on load voltage is shown in Figure 11, and the effect of slot width, slot body width, and slot depth on no-load voltage is shown in Figure 12. The generator performances before and after optimization are shown in Table 6.

Table 3. Genetic algorithm parameters.

Population Size	Maximum Genetic Algebra	Individual Length	Generation Gap	Cross Probability	Probability of Variation
40	50	40	0.95	0.7	0.01

Table 4. Value range of optimization variable.

Variable	δ/mm	L_1/mm	h_{Mp}/mm	b_0/mm	d_2/mm	h/mm
min	2.0	20.0	4.0	4.0	8.0	30.0
max	3.0	30.0	6.0	6.0	12.0	45.0

Table 5. Optimization results.

Variable	δ/mm	L_1/mm	h_{Mp}/mm	b_0/mm	d_2/mm	h/mm
Before optimization	2.5	25.0	5.0	5.0	10.0	35.0
After optimization	2.8	24.3	4.5	5.3	11.2	33.5

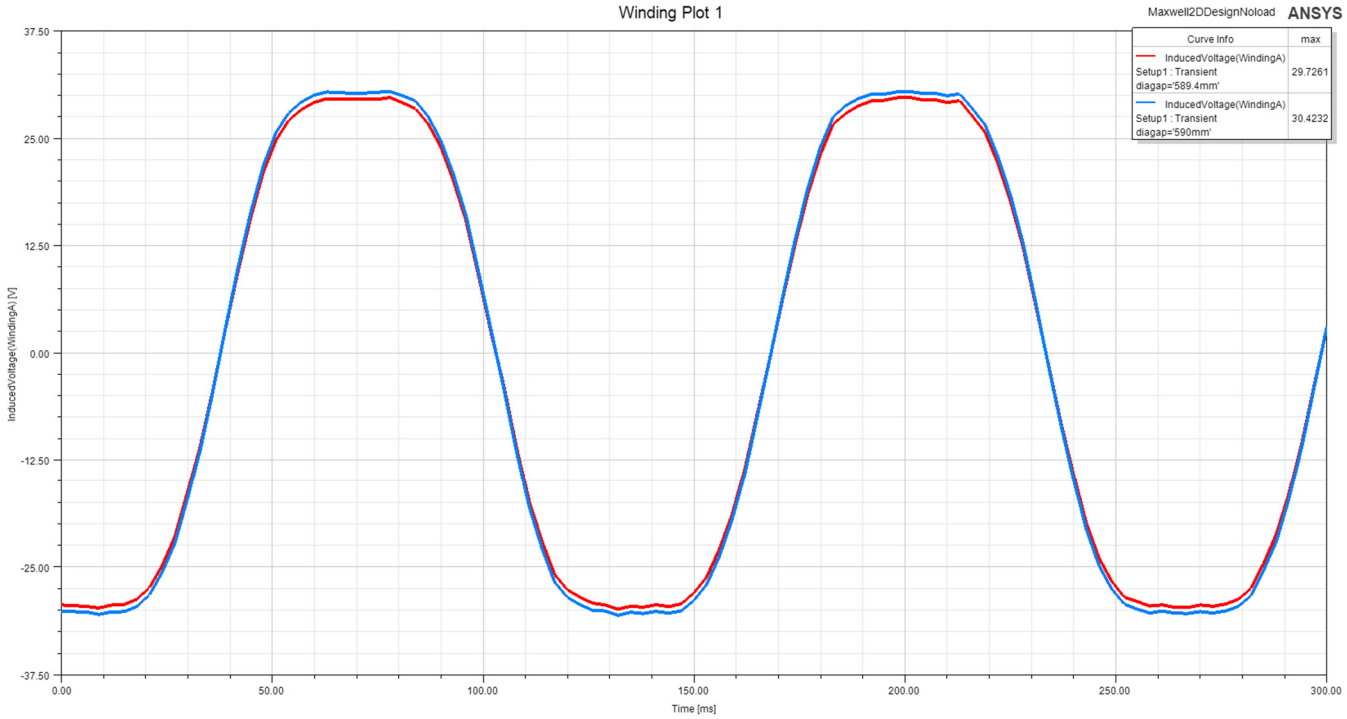

Figure 11. Effect of air gap length, iron core length, and permanent magnet thickness on load voltage.

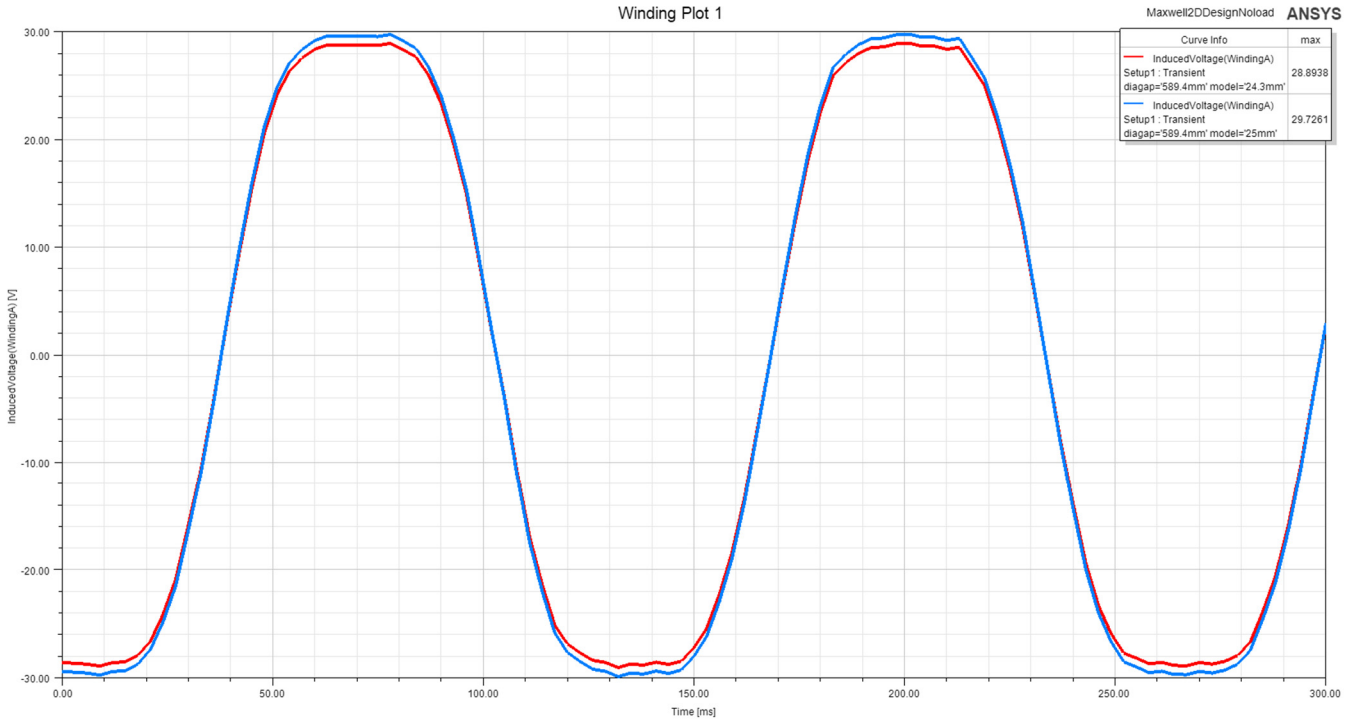

Figure 12. Influence of slot width, slot body width, and slot depth on no-load voltage.

Table 6. The motor performance before and after optimization.

Performance Index	Voltage Regulation Rate/%	Stator Tooth Magnetic Density/T	Stator Yoke Magnetic Density/T	Air Gap Magnetic Density/T
Before optimization	7.93	1.62	0.96	0.73
After optimization	6.85	1.82	0.98	0.84

Table 5 demonstrates that the air gap length, slot width, slot body width, and slot depth of the generator have all increased through optimization, while the iron core length and permanent magnet thickness have decreased. Figures 11 and 12 show that the load voltage and no-load voltage of the optimized generator have been reduced. Table 6 shows that the optimized generator stator tooth magnetic density, stator yoke magnetic density, and air gap magnetic density have all increased. The optimized generator voltage regulation has decreased 13.6% compared to the previous model, which confirms the effectiveness of the genetic optimization algorithm. Based on these optimization results, a prototype was produced for further drag experiments.

5. Actual Test of Underwater Generator

5.1. Generator Dragging Experiment

The generator dragging experiment took place at Hangzhou Jianghe Factory with the test temperature of 32.5 °C and the rate load of 20 Ω for the test system. Figure 13 displays a photo of the generator dragging experiment. As demonstrated in Figure 14, the generator began operating at a speed close to 5 rpm, and at the rated rotation speed of 28 rpm, the output power reached 121.3 W, which fulfilled the design requirements for rated power. The voltage regulation of the prototype obtained through no-load and rated load experiments is 7.05%, which is similar to the optimized simulation results.

Figure 13. Photo of the motor dragging experiment.

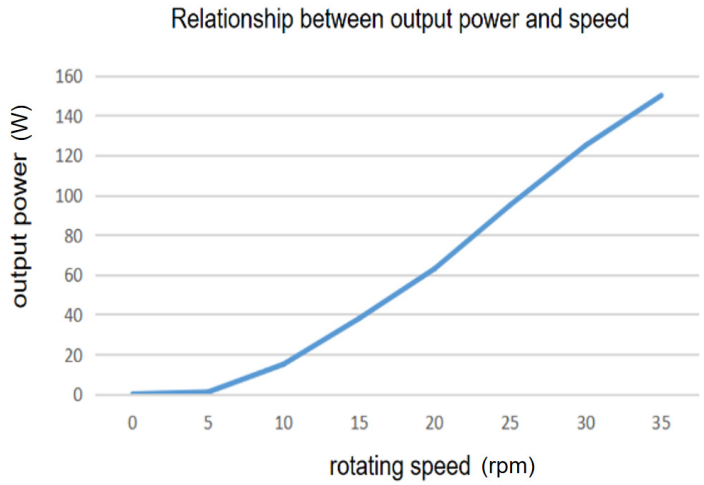

Figure 14. Measured output power.

5.2. Generator Sealing Experiment

The horizontal-axis tidal current generator operates in a seawater immersion environment, so its insulation and sealing performance determine the reliability of the generator's operation. The traditional horizontal-axis tidal current generator adopts a sealed cabin structure for sealing, and only a dynamic sealing structure is designed at the transmission shaft to ensure power transmission and underwater sealing of the generator. However, as the operating time of the generator increases, it is difficult for this method to ensure the reliability of the generator due to the inherent principle defects of dynamic sealing [21]. The heat generated during the full power operation of the generator causes the internal pressure in the sealed compartment of the generator to be greater than the external pressure, while during low-speed operation, the cooling of the generator causes the external pressure in the sealed compartment to be greater than the internal pressure, resulting in alternating large changes in pressure at the dynamic sealing area, causing seawater leakage and damaging the sealing reliability of the generator [22]. The prototype used polyurethane elastic resin for overall seals, and a certain thickness of polyurethane colloid is formed on the surface of the stator and rotor. The thickness of the stator outer surface adhesive layer is 1.0 to 2.0 mm, the inner surface adhesive layer of the stator is 5 mm, and the thickness of the adhesive layer at both ends of the stator is 10 mm, the surface adhesive layer of the stator is smooth and dense. After the sealing is completed (Figure 15), the underwater pressure test (Figure 16) was carried out on the generator. The stator and rotor of the generator were placed in an underwater pressure environment of 20 m, and the pressure tank was maintained at 0.3 MPa. After 52 h, the insulation resistance was greater than 5 M Ω, which meets the operational requirements for the horizontal-shaft tidal current energy underwater generator.

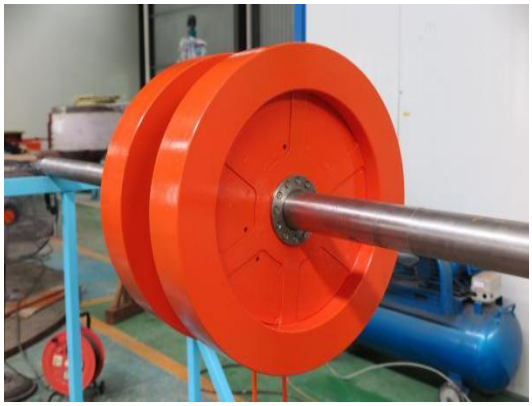

Figure 15. Photo of the generator after sealing.

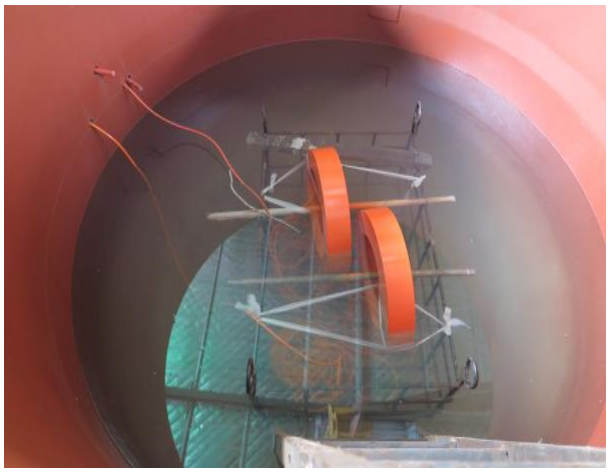

Figure 16. Photo of the generator sealing experiment.

5.3. Water Tank Dragging Experiment

After the sealing test, the generator and impeller have been assembled, and the water tank dragging experiment was conducted to simulate different water flow speeds by varying the forward speed of the trailer. Figures 17 and 18 depict the experimental setup and photos, respectively. The structure of the traction system mainly includes the traction platform, tidal current power generation device, circuit breaker, three-phase rectifier filter, programmable electronic load, and laptop monitoring and recording software. The circuit breaker is used to connect the front-end energy capture and generation system with the back-end energy conversion monitoring system; The three-phase sorting filter rectifies and filters the three-phase alternating current into a smoother direct current; programmable electronic loads are used to control the load output characteristics of power generation systems at different flow rates; laptops are used for real-time monitoring and recording of drag test data. The electronic load used for this test is the Feisi FT6300 series single programmable DC electronic load, which is set to constant resistance mode. Based on the calculation of the design parameters of the generator, the resistance values are set to 30 Ω, 35 Ω, and 40 Ω, with drag flow rates ranging from 0.2 m/s to 1.0 m/s and flow rate steps of 0.05 m/s. The cables for the power generation device and current meter are connected to the status monitoring system on shore. The generator output is connected to the battery charging and discharging module, which can monitor the generator's speed and electrical parameters during the charging and discharging process. The monitoring system hardware mainly consists of rectification, speed measurement module, power monitoring module, voltage reduction module, power supply module, battery, processing control unit, 4G communication transmission module, etc. The processing control unit obtains information such as speed, generator output voltage, current, frequency, temperature, depth, flow rate, flow direction, and underwater sound signals, and uploads this information to the cloud server through a 4G communication module. The monitoring data returned by the monitoring module is viewed on the server side of the monitoring system. The results of the water tank dragging experiment are shown in Table 7. When the flow rate was 0.25 m/s and the resistance was kept constant at 30 Ω, the system was started, and the generator's average output power was 3.5 W. At the flow rate of 0.8 m/s, the average output power of the generator was 122.31 W. The output voltage changed slightly when the load was changed, demonstrating the generator's suitability for low flow rate tidal current energy resources in China.

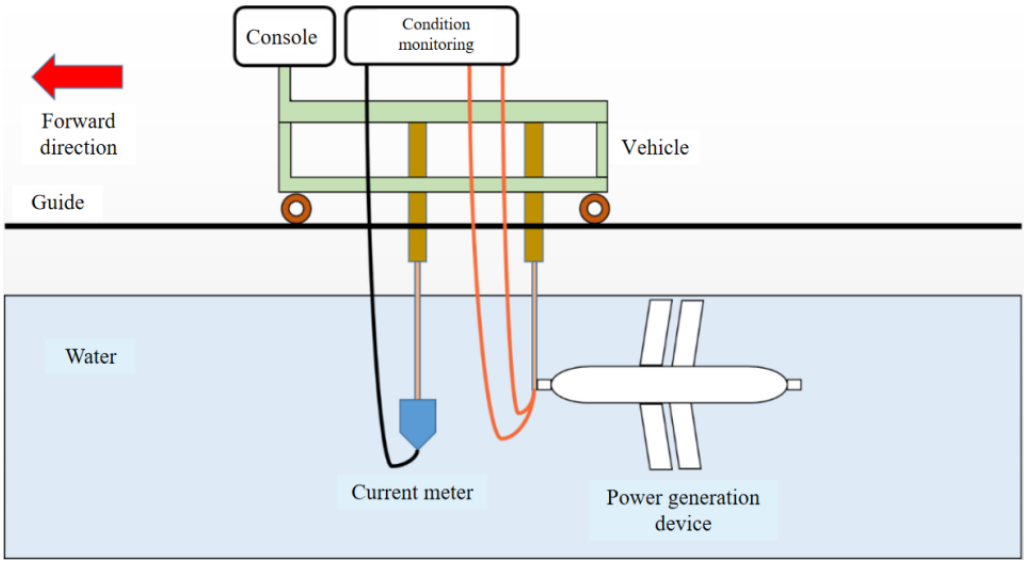

Figure 17. Schematic diagram of the dragging experiment.

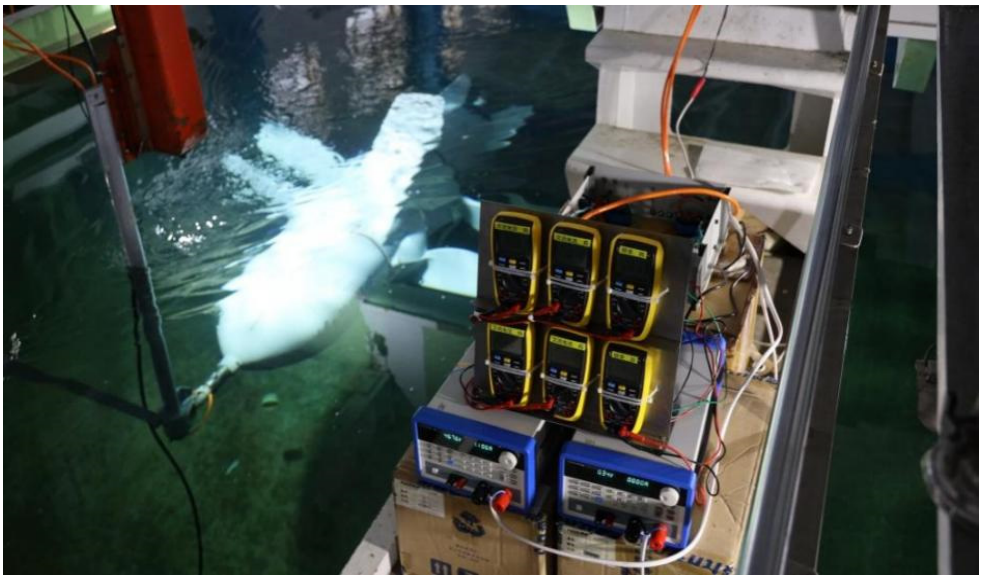

Figure 18. Photo of the dragging experiment.

Table 7. Water tank dragging experiment results.

Load/Ω	Start Flow Rate/m/s	Starting Power/W	Rated Flow Rate/m/s	Output Power/W	Output Voltage/V
30	0.25	3.65	0.88	123.85	38.74
35	0.25	3.56	0.90	123.18	37.21
40	0.26	3.49	0.91	122.31	36.52

6. Conclusions

This paper designed a 120 W, 28 rpm PMSG that can be used specifically for tidal current energy. The design formula is corrected based on the operating conditions. The design scheme is validated using finite element simulation. Further optimization is conducted using the genetic optimization algorithm to reduce the voltage regulation. After completing the design, a prototype is manufactured for a generator dragging experiment, underwater pressure test, and water tank dragging experiment. The experimental results

show that the prototype meets the design requirements, verifying the effectiveness of the generator design method proposed in this study. This provides a reference for the design of low-speed direct-drive PMSG for tidal current energy and lays a technical foundation for the long-term reliable operation of power generation devices using tidal current energy.

Author Contributions: Conceptualization, C.M.; Formal analysis, X.Z. (Xueming Zhang); Investigation, L.C.; Methodology, J.C.; Software, B.W.; Validation, X.Z. (Xiao Zhang); Writing—original draft, Y.Z.; Writing—review & editing, W.Z. All authors have read and agreed to the published version of the manuscript.

Funding: This research was funded by the international cooperation project of the Ministry of Science and Technology, grant number 2021YFE0107600; this research was also funded by Key R&D projects of Jilin Provincial Department of Science and Technology, grant number 20210203104SF, 20210402071GH.

Institutional Review Board Statement: Not applicable.

Informed Consent Statement: Not applicable.

Data Availability Statement: Some or all data, models, or code generated or used during the study are available from the corresponding author by request.

Conflicts of Interest: The authors declare no conflict of interest.

References

1. Tian, J.; Yu, L.; Xue, R.; Zhuang, S.; Shan, Y. Global low-carbon energy transition in the post-COVID-19 era. *Appl. Energy* **2022**, *307*, 118205. [CrossRef] [PubMed]
2. Jouffray, J.B.; Blasiak, R.; Norström, A.V.; Österblom, H.; Nyström, M. The blue acceleration: The trajectory of human expansion into the ocean. *One Earth* **2020**, *2*, 43–54. [CrossRef]
3. Khan, N.; Kalair, A.; Abas, N.; Haider, A. Review of ocean tidal, wave and thermal energy technologies. *Renew. Sustain. Energy Rev.* **2017**, *72*, 590–604. [CrossRef]
4. Eng, B.A.M.B. *Combined Experimental Testing and Numerical Modelling of a Novel Vertical Axis Tidal Turbine*; National University of Ireland: Galway, Ireland, 2018.
5. Zhang, Y.-L.; Lin, Z.; Liu, Q.-L. Marine renewable energy in China: Current status and perspectives. *Water Sci. Eng.* **2014**, *7*, 288–305.
6. Li, B.; Li, L.; Yang, L.; Yang, X.; Xiao, Y. Utilization and research status of tidal current energy. *Solar Energy* **2010**, *9*, 39–42.
7. Gu, Y. Study on the Key Technologies of the Grid-connected Marine Current Turbine's Control System. Ph.D. Thesis, Zhejiang University, Hangzhou, China, 2018.
8. Moury, S. *Design of Low Speed Axial Flux Permanent Magnet Generators for Marine Current Application*; Memorial University of Newfoundland: St. John's, NL, Canada, 2010.
9. Lindh, P.M.; Jussila, H.K.; Niemela, M.; Parviainen, A.; Pyrhonen, J. Comparison of concentrated winding permanent magnet motors with embedded and surface-mounted rotor magnets. *IEEE Trans. Magn.* **2009**, *45*, 2085–2089. [CrossRef]
10. Fizari, A.J.; Wijaya, F.D.; Cahyadi, A.I.; Adiyasa, I.W. Design and Simulation Permanent Magnet Synchronous Generator 1.5 kW for Ocean Current Turbine. In Proceedings of the 2019 IEEE Conference on Energy Conversion (CENCON), Yogyakarta, Indonesia, 16–17 October 2019; pp. 121–125.
11. Nikbakhsh, A.; Izadfar, H.; Beromi, Y. Design and optimization of permanent magnet synchronous generator for use in hydrodynamic renewable energy by applying ACO and FEA. *IIUM Eng. J.* **2017**, *18*, 158–176. [CrossRef]
12. Quintal-Palomo, R.; Dybkowski, M.; Gwoździewicz, M. Parametric analysis for the design of a 4 pole radial permanent magnet generator for small wind turbines. *Power Electron. Drives* **2016**, *1*, 175–186.
13. Faiz, J.; Valipour, Z.; Shokri-Kojouri, M.; Khan, M.A. Design of a Radial Flux Permanent Magnet Wind Generator with Low Coercive Force Magnets. In Proceedings of the 2016 2nd International Conference on Intelligent Energy and Power Systems (IEPS), Kyiv, Ukraine, 7–11 June 2016; pp. 1–7.
14. Hebala, A.; Ghoneim, W.A.; Ashour, H.A. Detailed Design Procedures for Low-Speed, Small-Scale, PMSG Direct-Driven by Wind Turbines. In Proceedings of the 2018 XIII International Conference on Electrical Machines (ICEM), Alexandroupoli, Greece, 3–6 September 2018; pp. 697–703.
15. Liwei, C.; Wenpeng, C.; Yinchao, L.; Shanguo, P.; Junsheng, W. Filling and sealing technology of ocean underwater generator. *Polyurethane Ind.* **2018**, *33*, 34–36.
16. Madani, N.; Cosic, A.; Sadarangani, C. A permanent magnet synchronous generator for a small scale vertical axis wind turbine. In Proceedings of the 2015 IEEE International Electric Machines & Drives Conference (IEMDC), Coeur d'Alene, ID, USA, 10–13 May 2015; pp. 48–52.

17. Madani, N. Design of a Permanent Magnet Synchronous Generator for a Vertical Axis Wind Turbine. Master's Thesis, Royal Institute of Technolgy, Stockholm, Sweden, December 2011.
18. Htet, T.Z.; Zhao, Z.; Gu, Q. Design Analysis of Direct-Driven PMSG in Wind Turbine Application. In Proceedings of the 2016 International Conference on System Reliability and Science (ICSRS), Paris, France, 15–18 November 2016; pp. 7–11.
19. Jeong, C.L.; Kim, Y.K.; Hur, J. Optimized design of PMSM with hybrid-type permanent magnet for improving performance and reliability. *IEEE Trans. Ind. Appl.* **2019**, *55*, 4692–4701. [CrossRef]
20. Li, W.; Cheng, M. Systems. Investigation of influence of winding structure on reliability of permanent magnet machines. *Trans. Electr. Mach. Syst.* **2020**, *4*, 87–95. [CrossRef]
21. Zhang, Z.; Zhang, Y.; Zheng, Y.; Zhang, J.; Fernandez-Rodriguez, E.; Zang, W.; Ji, R. Power fluctuation and wake characteristics of tidal stream turbine subjected to wave and current interaction. *Energy* **2023**, *264*, 126185. [CrossRef]
22. Zhang, Y.; Zang, W.; Zheng, J.; Cappietti, L.; Zhang, J.; Zheng, Y.; Fernandez-Rodriguez, E. The influence of waves propagating with the current on the wake of a tidal stream turbine. *Appl. Energy* **2021**, *290*, 116729. [CrossRef]